Ultrasound in Medicine & Biology 49 (2023) 1275–1287

Contents lists available at ScienceDirect

Ultrasound in Medicine & Biology

journal homepage: www.elsevier.com/locate/ultrasmedbio

Original Contribution

Ultrasound and Microbubbles Increase the Uptake of Platinum in Murine Orthotopic Pancreatic Tumors

Margrete Haram [a,b,c,*], Sofie Snipstad [c,d,e], Sigrid Berg [f], Patricia Mjønes [b,g], Elin Rønne [g], Jessica Lage [d], Melina Mühlenpfordt [d], Catharina De Lange Davies [d]

[a] Department of Radiology and Nuclear Medicine, St. Olav's Hospital–Trondheim University Hospital, Trondheim, Norway
[b] Department of Clinical and Molecular Medicine, Norwegian University of Science and Technology, Trondheim, Norway
[c] Cancer Clinic, St. Olav's Hospital–Trondheim University Hospital, Trondheim, Norway
[d] Department of Physics, Norwegian University of Science and Technology, Trondheim, Norway
[e] Department of Biotechnology and Nanomedicine, SINTEF Industry, Trondheim, Norway
[f] Department of Health Research, SINTEF Digital, Trondheim, Norway
[g] Department of Pathology, St. Olav's Hospital–Trondheim University Hospital, Trondheim, Norway

ARTICLE INFO

Keywords:
Pancreatic adenocarcinoma
Chemotherapy
FOLFIRINOX
Focused ultrasound
Microbubbles
Sonopermeation
Cavitation
Sonoporation
Drug delivery
Ultrasound contrast agents

Objective: Currently available cytotoxic treatments have limited effect on pancreatic ductal adenocarcinoma (PDAC) because desmoplastic stroma limits drug delivery. Efforts have been made to overcome these barriers by drug targeting the tumor microenvironment. Results so far are promising, but without clinical impact. Our aim was to investigate whether ultrasound and microbubbles could improve the uptake and therapeutic response of conventional chemotherapy.
Methods: Orthotopic pancreatic tumors growing in mice were treated with commercially available FOLFIRINOX (fluorouracil, irinotecan, oxaliplatin and calcium folinate) and SonoVue microbubbles combined with focused ultrasound. Tumor uptake of platinum (Pt) was measured by inductively coupled plasma mass spectroscopy (ICP-MS), and tumor volumes were measured by ultrasound imaging.
Discussion: Uptake of Pt, the active ingredient of oxaliplatin, was significantly increased after ultrasound treatment of orthotopic PDAC tumors. Multiple injections with FOLFIRONOX increased the amount of Pt in tumors. However, the enhanced accumulation did not improve therapeutic response. Increased uptake of Pt confirms that ultrasound and microbubbles have potential in clinical practice with existing drugs.
Conclusion: The lack of therapeutic response, despite increased uptake in tumor tissue, emphasizes the importance of studying how to overcome stromal barriers.

Introduction

Pancreatic ductal adenocarcinoma (PDAC) is an aggressive disease with an overall 5-y survival of 14.5% for men and 14.7% for women in Norway [1]. This makes it the cancer with the lowest survival among all cancers in Norway in the period 2016–2020. Globally, the overall 5-y survival rate is approximately 6%, ranging from 2% to 9% [2]. One important cause of low survival is delayed diagnosis caused by late onset of symptoms. Life-prolonging treatment with chemotherapy remains the only option for 80% of patients after diagnosis. In the group of patients with locally advanced disease at diagnosis, treatment with the combination regimen FOLFIRINOX (fluorouracil, irinotecan, oxaliplatin and calcium folinate) yields a median overall survival of 24.2 mo [3]. Patients with metastatic disease have median survivals of 11.1 and 6.7 mo when treated with FOLFIRINOX and gemcitabine, respectively [4,5]. Treatment failure in both the curative and palliative settings is closely related to chemoresistance. A general challenge with systemic chemotherapy is the low uptake of drugs into solid tumors—as little as 0.01% of systemically administered drugs reach their desired target [6]. The abnormal tumor microenvironment plays an important role in chemoresistance [7,8]. Tumor vasculature is disorganized and tortuous, lymphatic drainage is defective and interstitial tumor pressure is increased [9]. A hallmark of PDAC is desmoplastic stroma, which consists of fibroblasts, collagen fibers and inflammatory cells and creates an environment that contributes to limited delivery of drugs [10,11].

There has been no major improvement in treatment of PDAC the past 40 y [2], and there is a need to develop new treatment strategies. Increasing tumor uptake of therapeutic drugs, with resulting improved therapeutic effect, is a long-sought aim. Focused ultrasound (FUS) combined with microbubbles (MB) is a promising strategy, and increased tumor uptake and reduced tumor growth have been reported for various tumors growing in mice [12,13], including PDAC [14–18].

* Corresponding author. Department of Radiology and Nuclear Medicine, St. Olav's Hospital–Trondheim University Hospital, Prinsesse Kristinas Gate 3, 7030 Trondheim, Norway.
E-mail address: Margrete.Haram@stolav.no (M. Haram).

https://doi.org/10.1016/j.ultrasmedbio.2023.01.014
Received 10 October 2022; Revised 21 December 2022; Accepted 19 January 2023

Low-intensity ultrasound leads to linear oscillations of MB, referred to as stable cavitation. Increasing the acoustic pressure further will lead to non-linear behavior of MB and eventually inertial cavitation. The oscillating MB have mechanical effects such as shear stress on the vessel wall and microstreaming in the surrounding fluid. Oscillating MB can also push and pull cell membranes directly. Inertial cavitation can cause shock waves and jet streams [19–21]. Together these processes can increase vascular permeability, either paracellularly or transcellularly, and improve the penetration of drugs through the extracellular matrix (ECM) [22]. FUS can also generate acoustic radiation force because of the absorption and scattering of the ultrasound waves, corresponding to a loss of momentum of the wave, which is transferred to the tissue [21,23–25]. This will generate a force in the direction of the ultrasound wave that can cause acoustic streaming, shear stresses, tissue displacement and acoustic radiation force that can push MB toward the blood vessel wall. Thus, acoustic radiation force can also improve extravasation and penetration of drugs in the ECM [23,25,26].

A clinical study treating 10 PDAC patients with gemcitabine in combination with FUS and Sonovue reported good treatment tolerability and increased survival compared with historical controls [27]. The chemotherapeutic combination regimen FOLFIRINOX is the first choice for patients in the palliative setting today, with gemcitabine alone or in combination with nab-paclitaxel as alternatives for patients with decreased tolerability. At St. Olav's Hospital in Trondheim, Norway, we have an ongoing randomized controlled trial treating patients with pancreatic cancer with FOLFIRINOX and SonoVue combined with FUS (NCT04146441). To obtain more knowledge on the mechanism of action of FOLFIRINOX in combination with MB and ultrasound, the current pre-clinical study was performed. The aim was to investigate whether ultrasound and MB can increase the uptake of FOLFIRINOX in PDAC growing in mice and if any increased uptake would improve the therapeutic response. The tumor uptake of platinum (Pt) was measured by inductively coupled plasma mass spectroscopy (ICP-MS). Immunohistochemistry (IHC) on formalin-fixed paraffin-embedded tumor tissue was used to evaluate potential tissue damage. The volume of orthotopically growing PDAC tumors was measured by ultrasound imaging.

Methods

Mice and tumor implantation

All experiments were approved by the National Food Safety Authority and conducted according to the European Convention for the Protection of Vertebrates Used for Scientific Purposes. Female B6 albino mice 6–12 wk old and 20–30 g were supplied by Janvier Laboratories (Le Genest-Saint-Isle, France) or Charles River (Calco, Italy). Four to five mice were placed in individually ventilated cages with enrichment, nesting material and free access to food and water. Temperature and humidity were kept in the ranges 20°C–22°C and 50%–55%, respectively.

Murine pancreatic cells from the cell line KPC001S gLuc/green fluorescence protein were a kind gift from Steele Laboratories, Massachusetts General Hospital, Harvard University. Cells were cultured in Dulbecco's modified Eagle's medium (DMEM, Gibco Invitrogen, Carlsbad, CA, USA) supplemented with 10 % fetal bovine serum and 1% penicillin–streptomycin (both from Sigma Aldrich, St. Louis, MO, USA). The cells were grown until they reached ~60% confluence at 37°C and 5% CO_2.

Under gas anesthesia with 2% isoflurane in 40% O_2 and 60% NO_2, animals were placed on heating pads and their left hindlimbs shaved. For heterotopic tumor implantation, 0.2×10^6 cells suspended in 20 μL of 1:1 DMEM:matrigel (Sigma Aldrich) were injected slowly subcutaneously (s.c.) into the lateral aspect of the hindlimb.

Orthotopic implantation of cells was performed by laparotomy as described [28]. In addition to gas anesthesia, the animals were anesthetized locally in the area of incision with 0.04 mL of 10 mg/ml lidocaine (Accord Healthcare Limited, Middlesex, UK) and received 0.07 mL of buprenorphine 0.3 mg/mL (Indivior Europe Limited, Dublin, Ireland) and 0.1 mL of meloxicam 5 mg/mL (Boehringer Ingelheim, Rohrdorf, Germany) for analgesia s.c. in the neck area. A 5- to 10-mm incision was made in the skin a few millimeters anteriorly to the spleen. The peritoneum was incised with a 5 mm incision. The tail of the pancreas was exteriorized using forceps. Cells (0.2×10^6) in 20 μL of medium were injected into the pancreatic tail with a 30 gauge needle. The pancreatic tail was gently placed back into the abdominal cavity. The peritoneum was sutured with Vicryl 6.0 resorbable sutures (Ethicon, Somerville, NJ, USA). The skin was closed with EZ metal clips (Stoelting Co., Wood Doyle, IL, USA). Animals were placed separately in heated cages at 27°C for observation for post-operative complications. No animals were transferred to conventional cages before they were observed waking up and resuming normal behavior and activities such as grooming and eating. Metal clips in the skin were removed after 4 d.

Dose determination

The cytotoxicity of the drugs toward the KPC cell line was confirmed by AlamarBlue assay (Supplementary Section S.1, online only). To determine the optimal dose for therapeutic effect and tolerable toxicity, five doses of FOLFIRONOX were injected into mice with heterotopic tumors. The administration of FOLFIRINOX differed from clinical practice as all drugs were administered mixed in one vial as a bolus, whereas clinically the drugs are given sequentially as a 46-h infusion. On the basis of published results with a comparable tumor model [29], calcium folinate (Pfizer, Zaventem, Belgium), oxaliplatin (SUN Pharma, Hoofddorp, Netherlands), irinotecan (Accord Healthcare, Middlesex, UK) and fluorouracil (Accord Healthcare, Middlesex, UK) were mixed and 100 μL was injected using a 24-gauge lateral tail vain catheter. The doses used are given in Table 1 (doses A–C). Treatment was administered on days 9 and 13 after tumor cell inoculation. All animals were killed 19 d after inoculation. Next, an additional two doses of FOLFIRINOX were injected based on calculations from clinical doses given in established protocols at St. Olav's hospital to equivalent mouse doses using a converting table [30] (doses E and F, Table 1). Treatment was administered on days 9

Table 1
Doses of the drugs oxaliplatin, irinotecan, fluorouracil and calcium folinate in the FOLFIRINOX combination

Drug	Oxaliplatin (mg/kg)	Irinotecan (mg/kg)	Fluorouracil (mg/kg)	Calcium folinate (mg/kg)	No.
A	0.6	6.3	6.3	12.5	4
B	1.2	12.5	12.5	25	4
C	1.9	18.8	18.8	37.5	4
D	0	0	0	0	4
E	**5**	**12.5**	**25**	**25**	**5**
F	**10**	**25**	**50**	**50**	**5**
G	**0**	**0**	**0**	**0**	**4**

Doses of drugs A–C are based on published pre-clinical data [29]. Doses E and G (boldface) are calculated based on clinical doses from standard protocols at St. Olav's Hospital and by use of an established human–mouse converting table [30]. No. indicates number of mice in each group.

and 12 after tumor cell inoculation, at a mean tumor volume of 155 ± 42 mm^3. All remaining animals were killed on day 23. Both cohorts were compared with controls that received no treatment (rows D and G). Volumes of subcutaneously growing tumors were measured by caliper and calculated as $\pi lw^2/6$, where l is length and w is width of the tumor.

Ultrasound setup and treatment of PDAC in mice

A 1-MHz single-element transducer (Imasonic, Besançon, France) with a geometric focus at 120 mm was used. Pulses were given as a burst of 10,000 cycles with a repetition frequency of 0.25 Hz for a total duration of 7 min and mechanical index (MI) of 0.3 or 0.6. The signals were generated by a KEYSIGHT 33500B Waveform Generator (Agilent Technologies, La Jolla, CA, USA) and amplified with a 50-dB RF power amplifier (No. 21001, E&I Engineering, Anderson, SC, USA). The transducer was fixed at the bottom of a water tank pre-filled with de-gassed water. *In vivo* cavitation was detected with a 5 MHz unfocused transducer (Harisonic, 0.85 in diameter, 17-0512-P, Olympus, MA, USA), fixed to the side wall of the water tank, pointing towards the tumor and positioned at an angle to the transmitting ultrasound beam. The signal was recorded by an oscilloscope (LeCroy WaveRunner 44Xs, LeCroy Corp., Chestnut Ridge, NY, USA). Real-time display of the frequency response of the received acoustic signals enabled visual control of increase in harmonic signal levels, reflecting stable cavitation, and broadband signal level, reflecting inertial cavitation. The water tank was pre-heated to 34°C to prevent hypothermia, and a heating lamp was placed above the animal during treatment. A dose of 100 μL of FOLFIRINOX solution at concentrations listed in Table 1 was injected through a tail vein cannula. Shortly after, the animals were placed on a lid with acoustic absorbing material (Fig. 1). Mice were anesthetized with 2% isoflurane in medical air during the FUS treatment. For the heterotopically growing tumors, the hindlimb with the subcutaneous tumor was placed through a hole in the lid 190 mm from the transducer surface in the far field to ensure that the entire tumor would be sonicated. The beam widths at 190 mm were 6 and 10 mm at 3 and 6 dB, respectively. For the orthotopically growing tumor, a 10-mm-diameter circle was drawn around the scar after laparotomy. The mouse was placed with the encircled area resting on a water-filled pad immersed through a hole in the lid. The distance between tumor and transducer was approximately 210 mm, resulting in beam widths of 7.5 mm and 20.0 mm at 3 and 6 dB, respectively. A 50-μL bolus of SonoVue (Bracco International, Amsterdam, Netherlands) was given directly before the FUS treatment, and a second was given 3.5 min after the start of FUS treatment.

Acoustic parameter optimization

The potential biological effect in tissues caused by ultrasound and MB is dependent on the applied MI and pulse length. On the basis of previous experiments, we applied a constant pulse length of 10,000 cycles and tested MIs of 0.6 (n = 8) and of 0.3 (n = 8) in heterotopic PDAC tumors. These animals received FOLFIRINOX immediately before the administration of FUS + MB. Controls received FOLFIRINOX only (n = 4). Treatment was given on days 7, 10 and 14 after inoculation. Some animals met the defined humane endpoints during the treatment period and hence were killed at the corresponding times. All remaining animals were killed on day 24.

Therapeutic efficacy

After determining the dose of FOLFIRINOX to be used and optimal MI, the therapeutic effect of FOLFIRINOX combined with FUS and MB was studied. A group of animals (n = 24) were equally divided into three groups: (i) FOLFIRINOX + FUS + MB (n = 8); (ii) FOLFIRINOX only (n = 8); and (iii) control receiving no treatment (n = 8).

The timeline for treatments and tumor volume monitoring by ultrasound imaging is given in Figure 2. Tumor cells were injected orthotopically on day 1. Groups 1 and 2 were treated with FOLFIRINOX on days 8, 11, 14, 17 and 30. Group 1 received treatment with MB and FUS immediately after injection of FOLFIRINOX. Treatment was paused after the first four treatments because of toxicity and poor health status caused by tumor growth. Groups 1 and 2 were given a final FOLFIRINOX dose on day 30 for measurement of Pt uptake in tumors by ICP-MS.

Cavitation data were recorded to confirm the presence of MB in the sonicated area and detect stable or inertial cavitation. Post-processing of the recorded cavitation data was performed as presented by Snipstad et al. [12]. In brief, the broadband cavitation level at each transmitted burst was defined as the mean broadband signal level in the frequency ranges between the harmonic and superharmonic peaks in the frequency range 1.5 to 5 MHz (*i.e.,* 1.6–1.9, 2.1–2.4, 2.6–2.9, 3.1–3.4, 3.6–3.9, 4.1–4.4 and 4.6–4.9 MHz). In addition, spectrograms were calculated to differentiate between stable and inertial cavitation and display the cavitation signal level over the entire frequency range of interest over

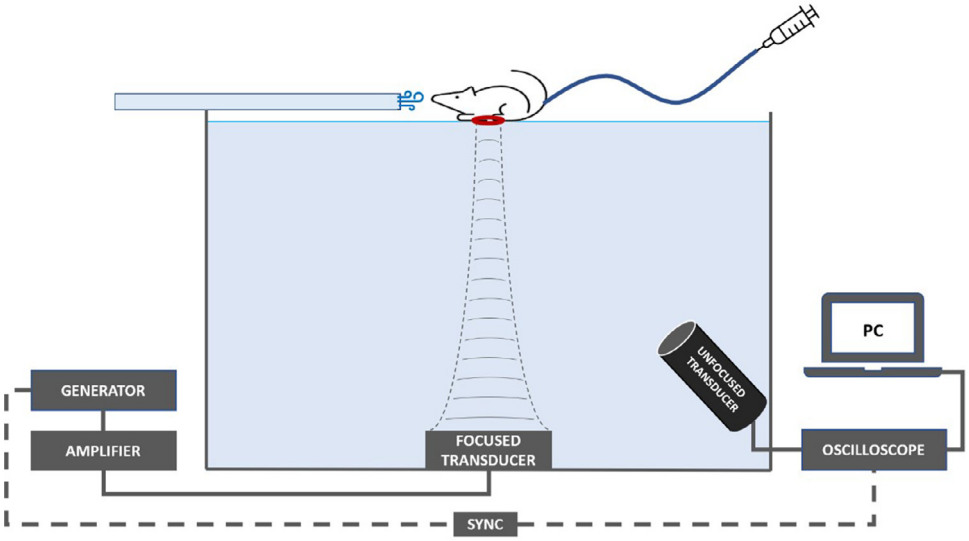

Figure 1. Schematic of the ultrasound setup. The ultrasound transducer placed at the bottom of a water tank was connected to an amplifier and signal generator. An unfocused transducer to the right was connected to an oscilloscope and PC for detection of cavitation signal. On the lid on top of the tank is a mouse receiving gas anesthesia. The *red circle* on the mouse indicates tumor. Drugs and microbubbles were administered by intravenous tail catheter.

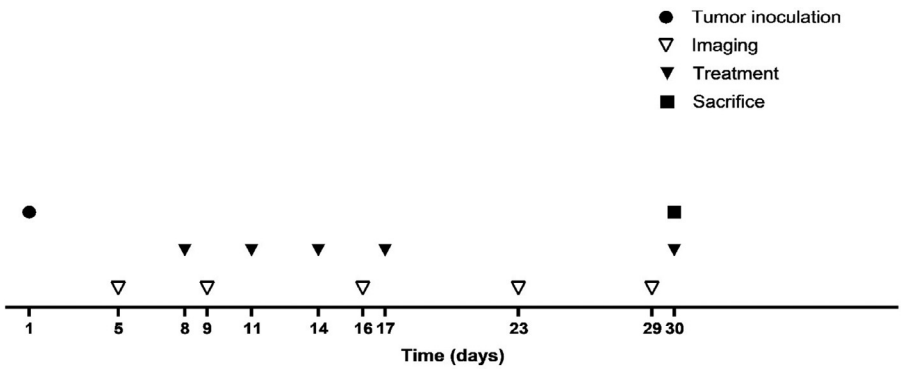

Figure 2. Timeline of tumor inoculation, ultrasound imaging, treatment and sacrifice of mice. KPC cell inoculation day 1. Imaging of all groups with ultrasound on days 5, 9, 16, 23 and 29. Treatment on days 8, 11, 14, 17 and 30. Treatment of group 1 (n = 8) with FOLFIRINOX, focused ultrasound and microbubbles. Treatment of group 2 (n = 8) with FOLFIRINOX. Controls (n = 8) received no treatment. All animals were killed on day 30.

time and were calculated using a moving Gaussian window of 10,000 samples and 50% overlap.

High-resolution ultrasound imaging and volume measurements

Volumes of orthotopic tumors were determined using a Vevo 3100 scanner (FUJIFILM, Visualsonics, ON, Canada) and an MX550 D probe with 40-MHz center frequency. This gives an in-plane resolution of 40 × 40 μm and 80 μm through-plane resolution. Volumes were calculated from step-size 76 μm, manually drawing tumor borders every fourth slice or 0.3 mm. All images were analyzed by the same investigator (M.H.). To account for intra-observer variability, all images were analyzed twice—first unblinded and then blinded for mouse ID, treatment groups and time of image acquisition.

Platinum tumor uptake by ICP-MS

Mice were treated on days 8, 11, 14, 17 and 30 with FOLFIFINOX ± FUS + MB (Fig. 2). Tumors were excised on day 30 after treatment, and Pt uptake was measured.

In a second study, we measured Pt uptake after a single treatment on day 18. Seventeen animals were inoculated with orthotopic PDAC-tumors. One mouse died, most probably because of anesthesia during surgery. On day 18, all mice received FOLFIRINOX treatment. Eight mice from different cages were randomly chosen to receive FUS + MB shortly after chemotherapy. After 2 h, all mice were killed by cervical dislocation and tumors excised.

Oxaliplatin is a small molecular drug with a molecular mass of 397.29 g/mol [31]. Its cytotoxicity is mediated through the formation of platinum–DNA adducts that inhibit DNA replication and transcription [32]; thus, Pt serves as a key component of the drug. In mice, total Pt has distribution and elimination half-lives of 2.3 and 49 min, respectively [32]. Tumors were excised 2 h after FUS treatment for Pt measurement. Tumor samples were weighed and stored at −80°C. After thawing, the samples were digested with 1.0 mL of ultrapure 65% 14.4 M HNO_3 produced from nitric acid (pro-analysis grade, VWR Corp., Radnor, PA, USA) using a quartz sub-boiling distillation system (SubPur, Milestone, Redding, CT, USA). Samples were heated at 105°C for 2 h. The digested samples were transferred into metal-free 50-mL polypropylene vials (VWR Corp.) and diluted to a final volume of 24 mL (24.4 g) with ultrapure water (PURELAB Option-Q, ELGA, Wycombe, UK) to a final acid concentration of 0.6 M HNO_3. Measurements with the Agilent 8800 triple quadrupole inductively coupled plasma mass spectrometry instrument (ICP-QQQ, Agilent Technologies, La Jolla, CA, USA) and calibration procedure is described in detail in Supplementary Section S.2 (online only).

Histopathology and immunohistochemistry

Orthotopic tumors were fixed in 4% formaldehyde and embedded in paraffin. Sections (4 μm thick) were stained with hematoxylin–erythrosine–saffron (HES); hematoxylin, erythrosine (both from Sigma Aldrich), Safran (VWR Corp.). Endothelial cells were stained using primary antibody CD31 (monoclonal IgG rabbit, 1:50 dilution, 60 min incubation) (Cell Signaling Technology, Danvers, MA, USA). Before application of the primary antibody, the sections were pretreated with Target Retrieval Solution, low pH (Dako, Carpinteria, CA, USA). The antibody was visualized using EnVision+ system horseradish peroxidase-labeled polymer anti-rabbit with 3,3′-diaminobenzidine+ (Dako), and subsequently counterstained with modified Gill's hematoxylin (Sigma Aldrich).

Statistics

Graphs and statistical calculations were performed with GraphPad Prism 8.0.1 (244) (GraphPad Software, San Diego, CA, USA). The Shapiro–Wilk test was applied for normality tests as a precondition for the application of an unpaired *t*-test. For statistical significance testing, two-tailed, unpaired *t*-tests with a significance level of $p < 0.05$ and 95% confidence interval were used. Welch's *t*-test was applied when groups had different standard deviations (SD). A Bland–Altman plot with log-transformed volumes was used to graphically reveal relationships between blinded and unblinded volume measurements.

Results

Dose determination

Mice with subcutaneous KPC tumors were given drugs intravenously at the concentrations =indicated in Table 1. There was no significant effect on tumor growth for any of the treated groups compared with controls (Fig. 3). No mice died during treatment in groups A–D. Mice receiving dose regimen E did not exhibit an increase in tumor volume when the drugs were given on days 9–12. However, the growth rate increased after the end of treatment. No mice in group E died during or after treatment. The death rate was 100% on day 21 in group F, which received the highest dose. In this group, three mice died, and two mice were killed because of weight loss. The death rate on day 21 was 50% in the control group (G) as a result of ulcerating tumors.

The mice receiving doses A–D did not lose any weight. Weight increased an average of 8.1% from days 8 to 15. In group E, the weight of the mice was reduced by only 3% on average between days 8 and 13. Group F, which received the highest dose, had an unacceptable average weight loss of 15% between days 8 and 13, and the weight decreased further to an average of 49% on day 20 when the remaining animals were killed because of humane endpoints. All mice except group F regained weight 10 d after the first injection of chemotherapy (Fig. 4).

On the basis of these toxicity observations, we decided to use the following doses: oxaliplatin 1. 5 mg/kg, irinotecan 12.5 mg/kg, fluorouracil 12.5 mg/kg and calcium folinate 25 mg/kg.

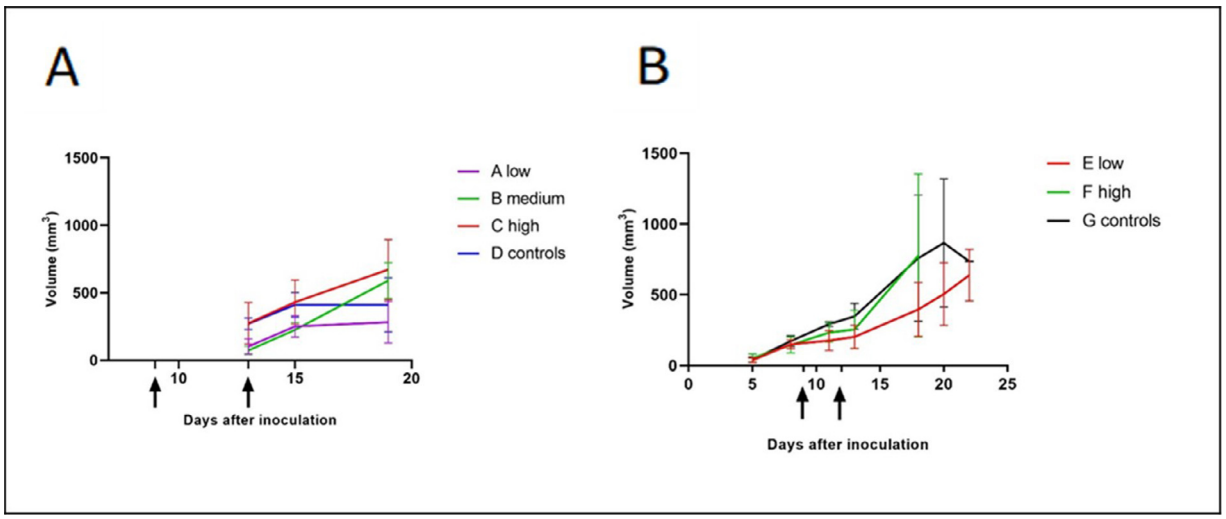

Figure 3. Tumor volume (mm^3) as a function of time. (A) Tumor volumes measured on days 13, 15 and 19 after KPC inoculation. Treatment was given on days 9 and 13 (*black arrows*). Increasing doses of FOLFIRINOX—*purple:* dose A low, (n = 4); *green:* dose B medium (n = 4); *red:* dose C high (n = 4); *blue:* dose D (no treatment, n = 4). (B) Tumor volumes measured days 5, 8, 11, 13, 18, 20 and 23 after KPC inoculation. Treatment was given on days 9 and 12 (*black arrows*). Increasing doses of FOLFIRINOX—*red:* dose E low (n = 5); *green:* dose F high (n = 5); *black:* dose G (no treatment, n = 4). Bars indicate standard deviation. Doses are given in Table 1.

Acoustic parameter optimization

To determine an MI that reduced tumor volume with limited tissue damage, MIs of 0.3 and 0.6 were compared. No significant difference in tumor growth was found between the groups treated with MI 0.3 and MI 0.6 although the tumors stopped growing during both treatments. There was a statistically significant reduction in growth in group MI 0.3 on days 14 and 17 and in group MI 0.6 on day 14 compared with controls (Fig. 5). This indicates a temporary therapeutic effect after three treatments. On the basis of previously published results from our group that revealed enhanced uptake of cabazitaxel in subcutaneously growing xenografts exposed to MB and MI 0.5 [12], we decided to use MI 0.6 in further experiments.

Therapeutic efficacy

After deciding on the dose of FOLFIRINOX and the MI for FUS treatment, the volumes of orthotopically growing tumors treated with FOLFIRINOX combined with FUS + MB and FOLFIRINOX alone and the untreated control were measured by 3-D ultrasound imaging. Tumor growth was infiltrative, affecting the pancreas, intestinal structures, visceral organs and abdominal wall. In many cases it became difficult, and in some cases impossible, to clearly delineate the tumor on days 23 and 29. The time point at which the tumors became impossible to delineate in a reproducible and precise way coincided with tumor volumes exceeding 500 mm^3. On day 29, this applied for 50% of tumors. Because reliable, reproducible measurements were not possible, these volumes were set to 500 mm^3. A significant proportion of tumors were also accompanied by carcinomatosis and ascites at late stages. In Figure 6A and 6B are examples of a well-circumscribed tumor anterior to the spleen in 2-D and 3-D, respectively, on day 28 after KPC inoculation. Figure 6C and 6D illustrate an infiltrating growing tumor.

The orthotopic PDAC tumor model failed to exhibit a therapeutic response to FOLFIRINOX either given alone or combined with FUS + MB. Neither the group treated with FOLFIRINOX combined with FUS + MB nor the group treated with FOLFIRINOX alone exhibited a

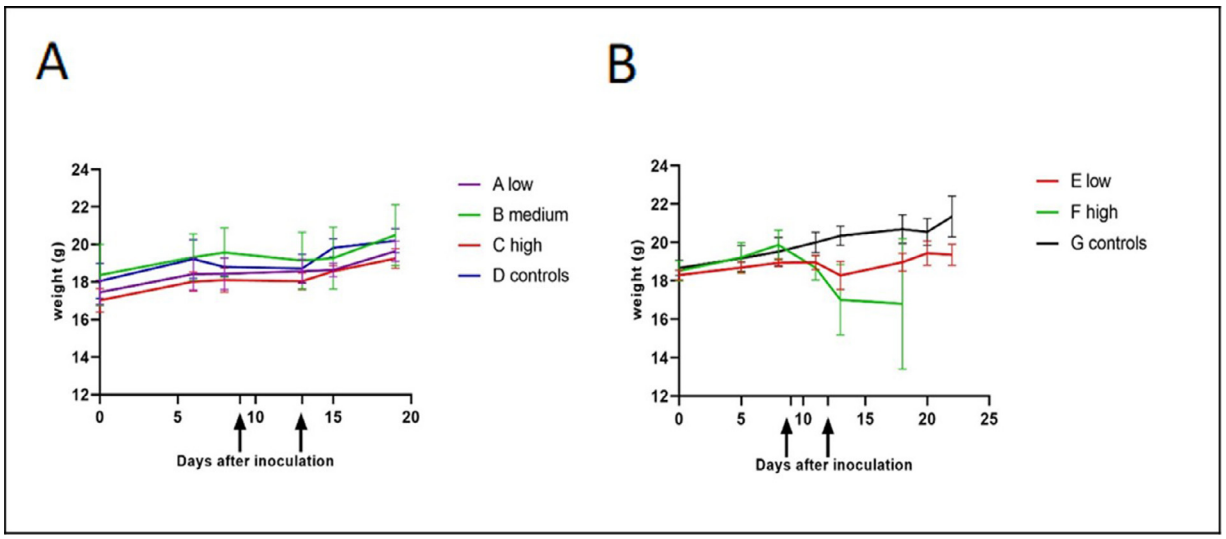

Figure 4. Body weight (g) as a function of time. (A) No significant weight loss on days 5–19 in groups A–D. *Purple:* dose A low (n = 4); *green:* dose B medium (n = 4); *red:* dose C high (n = 4); *blue:* dose D (no treatment, n = 4). Treatment with FOLFIRINOX was given on days 9 and 13 (*black arrows*). (B) Significant weight loss in dose group F from starting day 12. Treatment was given on days 9 and 12 (*black arrows*). *Red:* dose E low (n = 5); *green:* dose F high (n = 5–2); *black:* dose G (no treatment, n = 4). Bars indicate standard deviation. Doses A–C, E and F (mg/kg) of FOLFIRINOX are given in Table 1. MI, mechanical index.

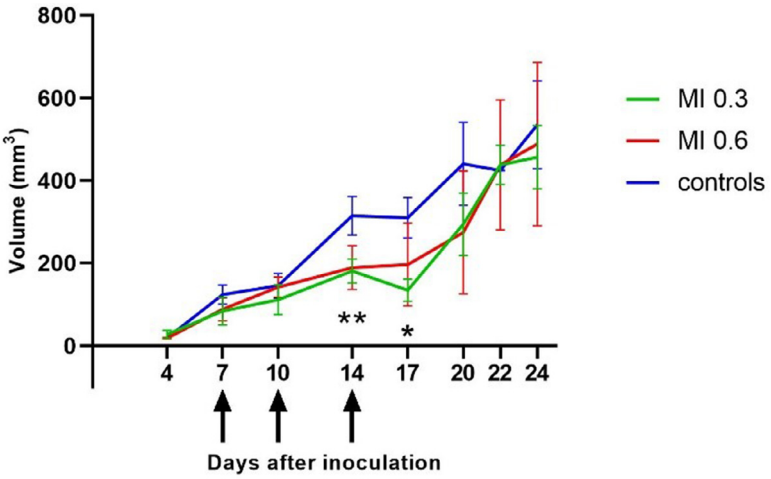

Figure 5. Mean tumor volume (mm^3) as a function of time. *Green:* MI 0.3; *red:* MI 0.6; *blue:* controls, no treatment. *Black arrows* indicate treatment days 7, 10 and 14. *Statistically significant difference compared with controls. On days 14 and 17, $p = 0.0012$ and 0.0003, respectively, for the MI 0.3 group. On day 14, $p = 0.003$ for the MI 0.6 group. Bars indicate standard deviations. MI, mechanical index.

statistically significant difference in tumor growth compared with untreated tumors (Fig. 7). There was large variation in tumor growth in all groups. In both groups receiving FOLFIRINOX, two of five mice seemed to respond to the treatment and had tumor volumes considerably smaller than 500 mm^3 after 29 d. However, two of the control tumors grew slowly, reaching sizes of only 66 and 72 mm^3 after 29 d. These animals also had the smallest tumors the first day the tumor could be imaged by ultrasound (day 9). In the group receiveing

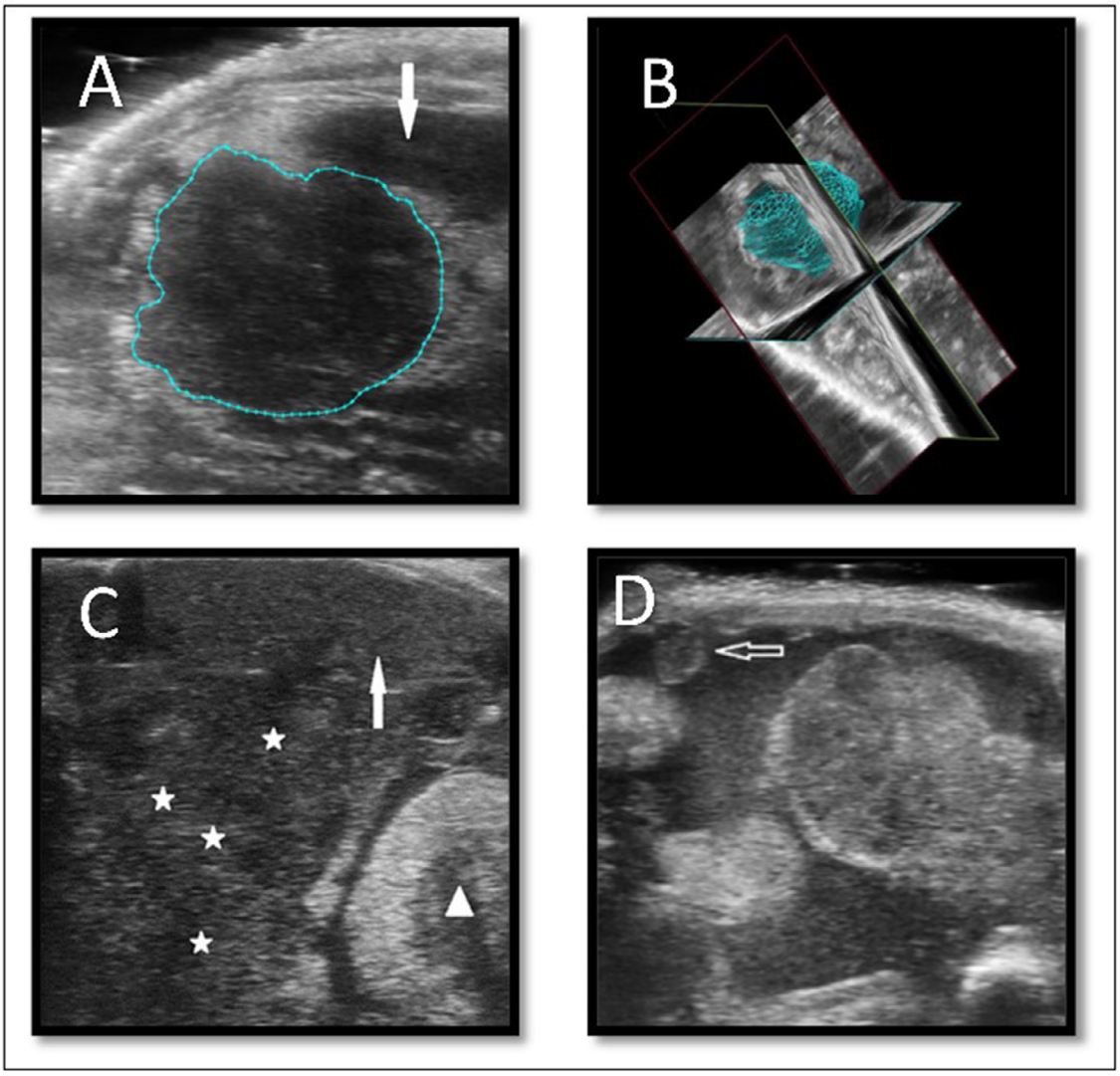

Figure 6. Two- and three-dimensional ultrasound imaging and volume measurement of pancreatic tumors. (A) Manual drawing of tumor on day 29 (*blue dotted line*). *Closed arrow:* spleen. (B) Three-dimensional reconstruction of tumor in image A. (C) Asterisks: tumor tissue on day 29, diffusely infiltrating intestinal structures. *Closed arrow:* spleen; *triangle:* kidney. (D) *Open arrow:* carcinomatosis with nodules along peritoneum. Ascites surrounding intestinal loops with tumorous tissue.

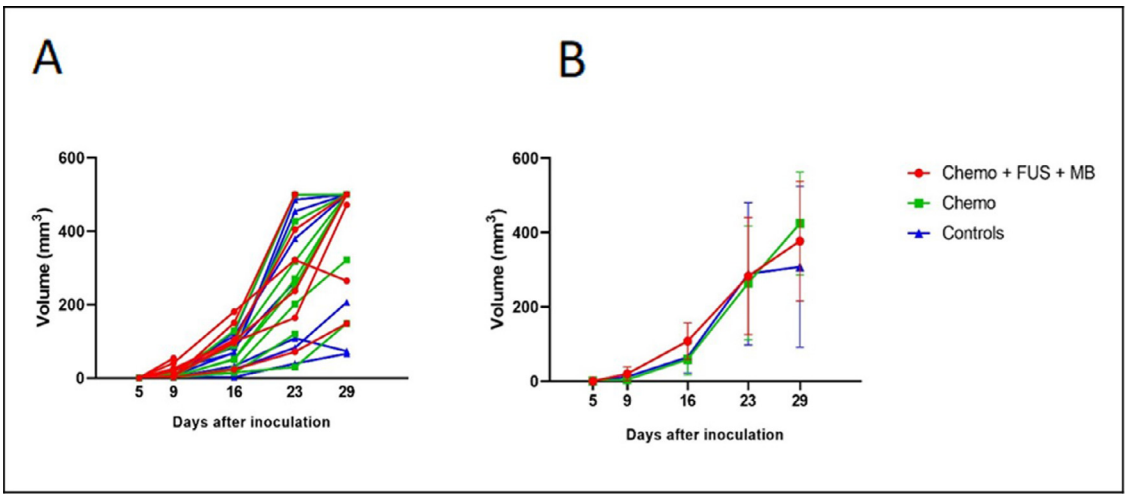

Figure 7. Tumor volume (mm^3) measured by ultrasound imaging as a function of time. (A) All individual tumors. Each line represents one mouse. (B) Volumes grouped as mean. Each data point is the mean of n = 8–5 mice. The groups received FOLFIRINOX + FUS + MB (*red,* n = 8–5) and FOLFIRINOX only (*green,* n = 8–7); controls received no treatment (*blue,* n = 8–6). All volumes are measure blinded for time and treatment groups. Treatment was given on days 8, 11, 14, 17 and 30. Bars indicate standard deviations. FUS, focused ultrasound; MB, microbubbles.

FOLFIRINOX combined with FUS + MB, three animals died spontaneously because of tumor burden and/or treatment toxicity before the last treatment on day 30. One mouse died in anesthesia during the final treatment on day 30. In the FOLFIRINOX-only group, two animals were sacrified at humane endpoints and one animal died from tumor burden and/or toxicity before the last treatment on day 30. In the control group, one animal died from tumor burden and three were sacrified at humane endpoints before day 30. Mice in all groups, independent of the treatment given, developed ascites. Between days 21 and 30, weight was stable or slightly increased in all groups. This indicates that weight is a poor marker for mice with orthotopic PDAC having ascites and that their health status was due to both tumor burden and toxicity.

Determining the tumor volume based on ultrasound imaging can be challenging because of infiltrating growth; thus, intra-observer variability was compared between unblinded and blinded measurements. Figure 8 is a Bland–Altman plot expressing difference between blinded and unblinded versus average of blinded and unblinded. A bias of 1.03 mm^3 indicates low and acceptable intra-observer variability. Blinded measurements are on average 3% larger than unblinded, and the plot reveals larger differences at early, low-volume measurements.

Cavitation data

Cavitation activity was recorded during FUS + MB treatment. Figure 9A illustrates an example of the increase in broadband cavitation signal as a function of time during treatment on day 14. The presence of cavitation signal indicates that MB injection was successful in all animals. The signal increase after each bolus injection typically lasted 50–70 s. Figure 9B illustrates cavitation signals during the final treatment on day 30. The mouse indicated by the *blue line* lacked cavitation signal because of a failed intravenous MB injection. Because of the failure to achieve cavitation, this mouse was excluded from calculations of Pt uptake.

The combination of a general increase in broadband noise level and peaks at the subharmonic (0.5 MHz) and superharmonic (1.5 MHz) levels indicates that there was a combination of inertial and stable cavitation (Fig. 9C). The spectrogram in Figure S2 (online only) reveals an example of the frequency content as a function of time from the treatment of one typical mouse on treatment day 14.

Platinum uptake in PDAC tumor

Although FUS + MB did not improve the therapeutic response of FOLFIRINOX, it was of interest to determine whether FUS + MB increased the uptake of drugs into the tumor tissue. Tumors were excised from the mice killed on day 30, and the amount of Pt was measured by ICP-MS. FUS + MB increased the amount of Pt on average approximately 2.5 times compared with the mice that received only FOLFIRINOX. There was a large variation in the amount of Pt detected, but the difference between the two groups is statistically significant

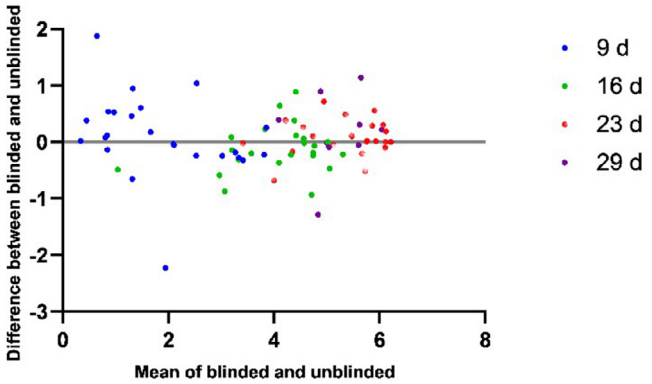

Figure 8. Bland–Altman plot expressing difference between blinded and unblinded volume measurements as a function of the average of the two measurements. Each symbol represents one tumor. $Y = 0$ indicates no difference between measurements. Measurements at 9 d (*blue*), 16 d (*green*), 23 d (*red*) and 29 d (*purple*). Volumes are log-transformed. Estimated relationship between blinded and unblinded is 1.03 mm^3 calculated back to original scale.

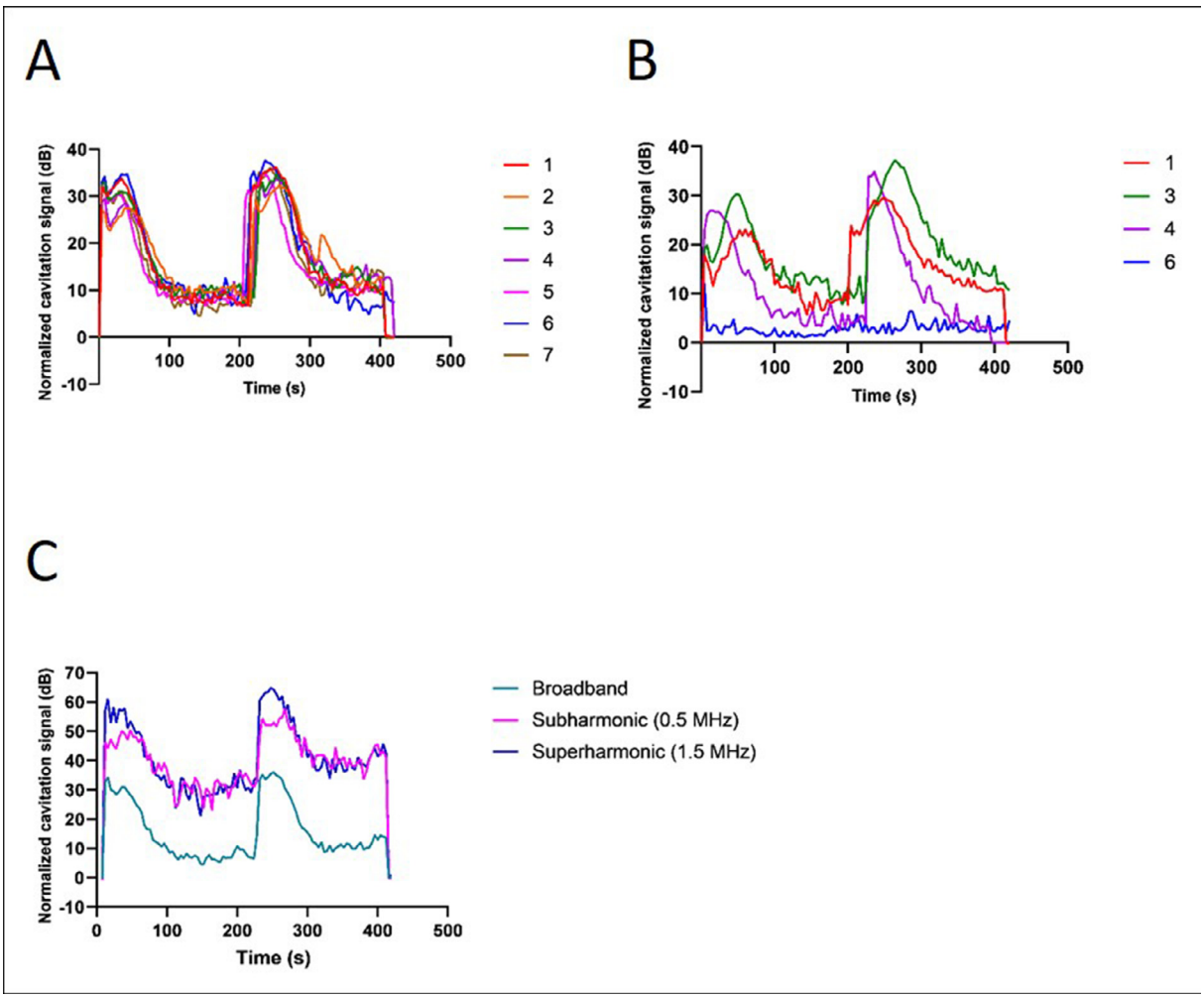

Figure 9. Cavitation signal. (A) Example of broadband cavitation signal from all individuals treated on day 14 expressed as signal increase from general noise floor (dB) as a function of time. (B) Broadband signals from all animals on the final treatment day. The final treatment on day 30 was successful in all animals except for mouse indicated in *dark blue* because of failure of intravenous cannulation; hence it was excluded from calculations of platinum uptake. Individual mice are represented by separate colors. (C) Example from treatment of one mouse on day 14 showing subharmonic (0.5 MHz, *pink*) and superharmonic (1.5 MHz, *dark blue*) signals in addition to broadband (*light blue*) signals. Noise floor is corrected by +132.5 dB in all graphs.

($p = 0.0470$) (Fig. 10A). Interestingly, the tumor sample from the mouse that failed intravenous MB injection (broadband signal in Fig. 9B) had a Pt concentration in the same range as the FOLFIRINOX-only group (158 μg/g). This tumor sample was excluded from calculations.

We observed a small amount of Pt in one of the tumors in the control group (Fig. 10A, *blue dots*). This might be caused by contamination during handling of the sample.

Increased uptake of Pt was measured on day 30, after five treatments. We wanted to investigate to what extent one single treatment increased uptake. Figure 10B reveals significantly increased uptake of Pt in PDAC tumors treated only once (day 18) with FUS + MB combined with FOLFIRINOX compared with tumors treated only with FOLFIRINOX. A 1.2-fold increase was detected, indicating that multiple treatments have an accumulative effect on the tumor uptake of FOLFIRINOX.

Histology: HES and CD31 staining

The HES staining of orthotopic PDAC tumors reveals that all tumors appear poorly differentiated and aggressive with dense tumor tissue (Fig. 11). Surprisingly, there was sparse connective tissue and connective tissue reaction. Desmoplasia, described as a prominent feature of PDAC in humans [33], was not dominating. Connective tissue reaction was at a minimum and not categorized as desmoplasia by experienced pathologists. Tumors were characterized by diffuse or solid growth. By visual inspection of all tumors, there was no detectable difference in general appearance, amount of necrosis, bleeding or vessel density between the groups receiving FOLFIRINOX combined with FUS + MB and FOLFIRINOX only or no treatment. No increased bleeding in treated tumors indicates that the parameters used were safe.

The CD31 staining of endothelial cells revealed poor vascularization of the PDAC tumors (Fig. 12). Generally, there was sparse vascularization centrally compared with peripherally. Central vessels also appeared thinner, elongated and dysmorphic compared with vessels in the periphery. This trait is in accordance with rapid tumor growth. Necrosis was frequently seen in central parts of the tumor, resulting from poor vascularization and impaired nutritional supply.

Discussion

A prerequisite for successful chemotherapy is that the drugs reach all tumor cells. The drugs should have an adequately long circulation time and not be degraded in the blood, be able to efficiently extravasate across the capillary wall and penetrate through the ECM without being hindered by the ECM constituents or stroma cells. Finally, the drugs need to be internalized into all tumor cells and reach their final intracellular target. To improve therapeutic response, all these steps need to be considered [34]. A well-known challenge in cancer therapy is low uptake of systemically injected drugs into solid tumors [6]. This applies

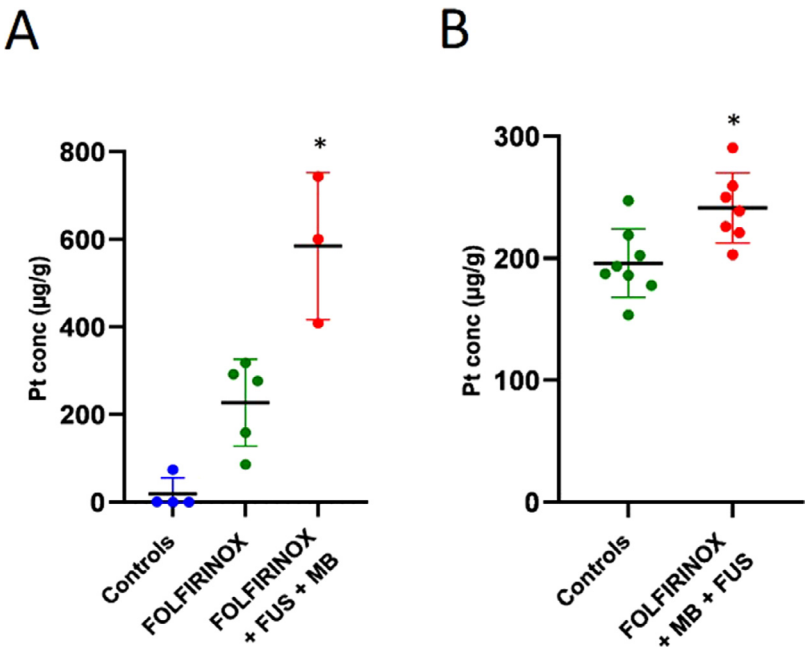

Figure 10. Tumor uptake of platinum. (A) Platinum concentration (µg/g) in tumor tissue after five treatments. Tumors were extirpated 2 h after final treatment on day 30. Control (*blue*), FOLFIRINOX (*green*). FOLFIRINOX and FUS + MB (*red*). Two-tailed *t*-test comparing FOLFIRINOX and FUS + MB with FOLFIRINOX only reveals a statistically significant difference with $p = 0.0470$. (B) Platinum concentration (µg/g) 2 h after one single treatment of FOLFIRINOX only (*green*) or FOLFIRINOX combined with FUS + MB (*red*), with a statistically significantly higher concentration of platinum after FUS + MB ($p = 0.0085$). Each symbol represents one tumor. The *black horizontal line* represents the mean, and the *error bar* is the standard deviation. *Statistically significant. FUS, focused ultrasound; MB, microbubbles; Pt, platinum.

particularly for PDAC, characterized by dense, desmoplastic tumor stroma and marked peritumoral fibrosis [33]. This is closely linked to chemoresistance [7] and is an important reason for the poor therapeutic response to FOLFIRINOX of patients with PDAC in adjuvant and palliative settings. Thus, in the present work, we investigated whether FUS + MB could enhance the tumor uptake of FOLFIRINOX and improve therapeutic response.

FUS + MB increased tumor uptake of Pt. Pt is an essential part of oxaliplatin and can be measured with ICP-MS. Five treatments increased the average uptake 2.5-fold, while a single treatment increased the uptake 1.2-fold, suggesting that a fraction of the drug resides in the tumor between treatments and allows for drug accumulation in the tumor. In accordance with our data, accumulation of nanoparticles after three repeated treatments with US + MB was reported by Snipstad et al. [12]. This indicates the need for multiple treatments.

Cavitation activity was detected by an unfocused listening transducer connected to an oscilloscope, and the cavitation reflects oscillating MB. Oscillating MB produce shear forces on the vessel wall causing either paracellular or transcellular extravasation [19,20,23,26,35], which can explain the improved tumor uptake of Pt. Oscillating MB might also cause the vessel wall to oscillate, inducing acoustic streaming thereby improving penetration into ECM [36,37]. However, the distribution of Pt in the ECM was not measured. Several studies have investigated the effect of FUS on the distribution of fluorescent dyes or fluorescent nanoparticles [38–40] and determined enhanced tumor uptake and improved distribution of the dye in the ECM. Fluorescent molecules and nanoparticles might behave differently than drug and drug-loaded nanoparticles; thus, we rather measured tumor uptake of Pt, not using a fluorescent substitute. We had previously determined that labeling nanoparticles with dyes changes nanoparticle properties [41].

The lack of therapeutic response of both FOLFIRINOX combined with FUS and MB and FOLFIRINOX alone can partly be explained by very aggressive, infiltrating tumor growth in the orthotopic PDAC model. Initially, we determined that the KPC001S gLuc cell line is susceptible to both the combined regimen FOLFIRINOX and single drugs *in vitro*. It is well known that although anticancer drugs may be able to kill tumor cells grown *in vitro*, they are unable to reach all tumor cells deep inside solid tumors [7,8,10,11,42]. The tumor cells that escape the cytotoxic effects of anticancer drugs will effectively be able to regenerate the tumors *in vivo* [43]. Numerous abnormalities in the microenvironment of tumors have been identified. By CD31 staining, we identified dysmorphic and very few endothelial cells in central parts of the tumors, limiting the access of drugs to this part of the tumor. This finding is accordance with known pathologic traits of human PDAC. Rapid cellular regeneration in central parts of the tumors also contributes to compression of blood vessels. The three main constituents of the ECM are collagen fibers, proteoglycans and glycosaminoglycans like hyaluronan [44,45]. These constituents create a network that acts as a barrier. Cancer-associated fibroblasts (CAFs) are the main cells responsible for changing the ECM composition of the tumor stroma. Through interaction with tumor cells, CAFs can upregulate production of ECM components and induce overexpression of ECM constituents, resulting in denser and stiffer tumor stroma compared with normal tissue known as desmoplasia. Rapid tumor growth and dense ECM lead to increased interstitial tumor pressure and solid stress. Solid stress develops when cancer cells, stromal cells, collagen fibers and other constituents of the ECM increase within a restricted environment [46]. Solid stress compresses both blood and lymphatic vessels, reducing tumor drainage leading to increased interstitial fluid pressure, limiting both vascular and interstitial transport [34]. Typical traits of desmoplasia were absent in histology sections from our orthotopic tumors. This finding is in contrast to human PDAC, but is in accordance with findings in orthotopic tumors in mice [29]. The orthotopic tumor model was nevertheless expected to mimic conditions in the microenvironment better than heterotopic models. Dense tumor tissue and sparse vascularization still effectively restricted drug access to tumor. Lack of treatment effect might be caused by failure in the final transport step to penetrate ECM to central parts of the tumor. Our finding of increased Pt uptake in tumors without effective therapeutic response supports the idea of the ECM as a significant barrier.

In this study, all drugs in the FOLFIRINOX combination were injected mixed in one vial according to Erstad et al. [29], who reported significant reduction in orthotopic tumor volume after FOLFIRINOX treatment. Oxaliplatin is partly hydrolyzed at basic pH and should ideally not be mixed with basic solutions [32]. Thus, mixing oxaliplatin with basic fluorouracil might have reduced its therapeutic effect without reducing the presence of the Pt metal component.

It is plausible that the other small molecular drugs in the FOLFIRINOX cocktail, 5-fluorouracil [47] and irinotecan [48], would follow the same pattern of tumor uptake as oxaliplatin subjected to the same FUS conditions.

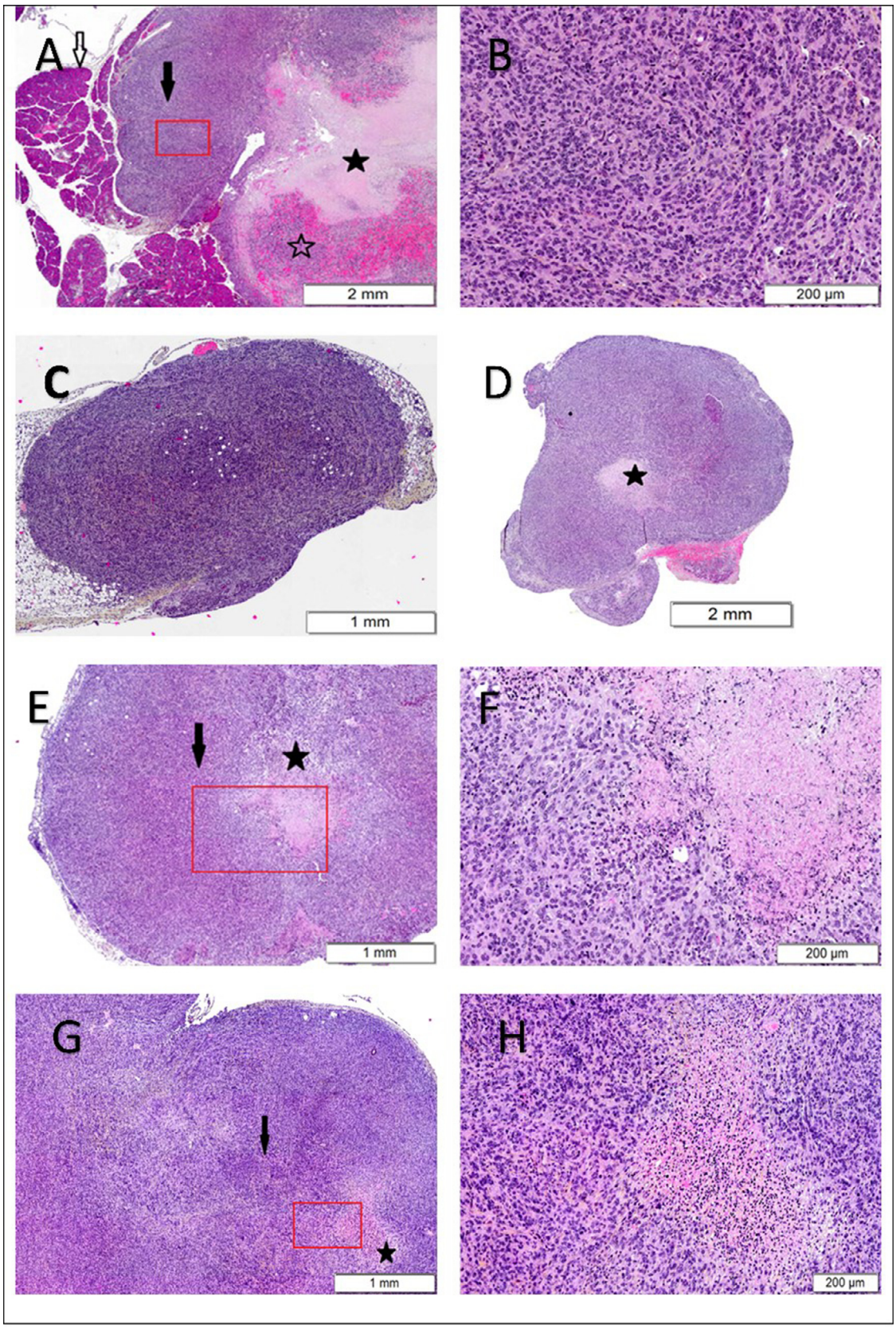

Figure 11. HES staining of orthotopic tumors revealing poorly differentiated tumors with solid growth. *Open arrows:* normal exocrine glands; *closed arrows:* tumor tissue; *closed stars:* necrosis; *open star*: bleeding. (A) Tumor treated with FOLFIRINOX and MB + FUS. (B) Section from (A, *red square*) with densely packed tumor cells. (C) Tumor treated with FOLFIRINOX and MB with densely packed tumor cells and no necrosis. (D) Tumor treated with FOLFIRINOX and MB with dense tumor and central necrosis. (E) Tumor treated with FOLFIRINOX only. (F) Section from (E) with dense tumor cells and necrosis (*light pink*). (G) Tumor in control group (no treatment) with densely packed tumor cells and necrosis. (H) Section from (G, *red square*) with densely packed tumor cells and area of necrosis (*pink*). Bars in right lower corners indicate magnification. FUS, focused ultrasound; HES, hematoxylin–erythrosine–saffron; MB, microbubbles.

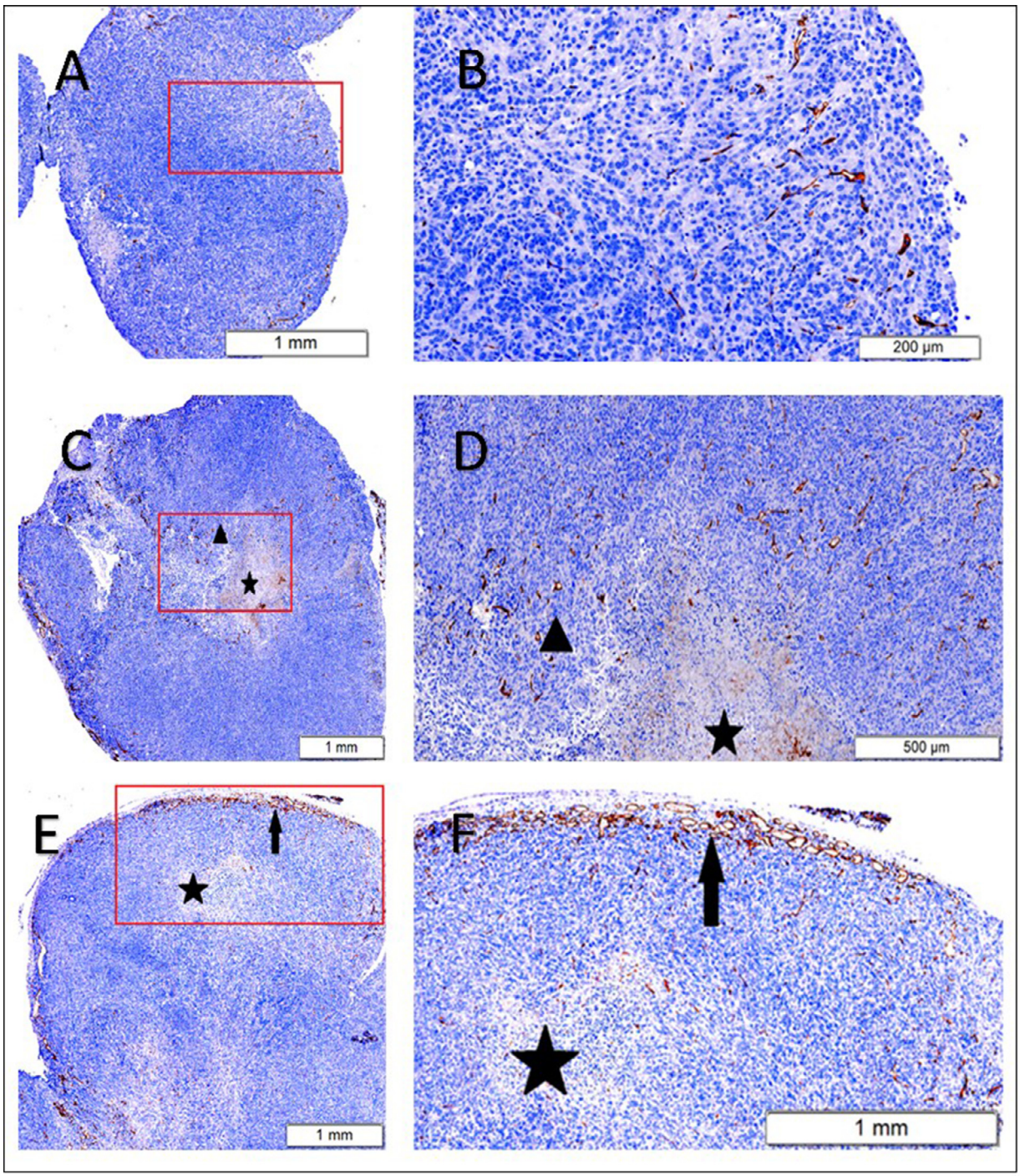

Figure 12. CD31-stained tumor sections revealing poorly vascularized tumors. Endothelial cells are stained *brown* (peroxidase). *Triangles*: endothelial cells; *stars*: necrosis; *closed arrow*: serosal lining. (A) Tumor treated with FOLFIRINOX and MB + FUS. (B) Section from (A, *red square*) revealing brown endothelial cells in the periphery of the tumor. (C) Tumor treated with FOLFIRINOX only, central necrosis. There is increased vascularization close to the necrotic area in the center. (D) Section of (C, *red square*) revealing endothelial cells in the periphery of necrosis. (E) Tumor in control group (no treatment) with poor vascularization centrally, areas of necrosis and an outer rim of tumor with vascularized serosal lining. (F) Section from (E, *red square*).

The resulting tumor burden and clinical picture differed within the same treatment groups, in accordance with clinical observations. PDAC is a heterogeneous disease with respect to genetics, pathology and clinical presentation and prognosis also in humans [33,49]. Oncologists observe large variations in clinical disease courses despite apparently similar starting points at diagnosis.

Successful oncologic treatment with chemotherapy requires optimal balance between dose and toxicity combined with supportive care. The first response evaluation of FOLFIRINOX treatment in the clinic is normally performed 8 wk after treatment start, and dose adjustments are frequently necessary. Our tumor model with aggressive disease and the application of humane endpoints allowed for no long-term follow-up. Genetically modified mice developing spontaneous tumors or a patient-derived xenograft model might exhibit slower tumor growth and reflect clinical pancreatic tumors to a larger extent than the KPC tumor.

The ultrasound parameters (frequency, acoustic pressure, pulse length, pulse repetition frequency and overall exposure time) applied vary between pre-clinical studies, and FUS may also be combined with

MB having differing properties. Choosing optimal FUS parameters and achieving improved therapeutic response and limited tissue damage are undergoing extensive pre-clinical research [14–17] and would benefit from standardization through interdisciplinary and international cooperation.

Conclusions

Our PDAC tumor model exhibited increased uptake of Pt, reflecting increased uptake of oxaliplatin in mice treated with a combination of FOLFIRINOX, FUS and MB compared with those receiving only FOLFIRINOX. To the best of our knowledge, this is the first study to determine that FUS and MB increase the uptake of FOLFIRINOX in a murine orthotopic tumor model. Improved therapeutic response in orthotopic tumors was not demonstrated, emphasizing the importance of ECM as a barrier to successful drug delivery and therapeutic response. FUS + MB is safe, simple, non-invasive and highly relevant for future clinical practice. Increased uptake of cytostatic drugs can be achieved with clinically well-proven, commercially available low-cost drugs and MB in combination with ultrasound. More research is crucial to understand the mechanisms underlying drug distribution in the setting of FUS-enhanced uptake to overcome ECM as a barrier.

Conflict of interest

The authors declare no competing interests.

Acknowledgments

We acknowledge Senior Engineer Ingunn Nervik at the Department of Clinical and Molecular Medicine, Norwegian University of Science and Technology (NTNU), for technical expertise in sectioning and histological staining; Senior Engineer PhD Anica Simic, Institute of Chemistry, NTNU, for technical expertise in ICP-MS analysis; Engineer PhD Kristin Grendstad, Institute of Physics, NTNU, for technical support in cell culturing; and the Department of Comparative Medicine (CoMed), NTNU, for housing and care of animals.

This work was funded by the Central Norway Regional Health Authorities.

Data availability statement

The research data for this article are available and can be accessed on request.

Supplementary materials

Supplementary material associated with this article can be found, in the online version, at doi:10.1016/j.ultrasmedbio.2023.01.014.

References

[1] Cancer Registry of Norway. Cancer in Norway 2020: cancer incidence, mortality, survival and prevalence in Norway. Oslo: Author; 2021.
[2] Ilic M, Ilic I. Epidemiology of pancreatic cancer. World J Gastroenterol 2016;22:9694–705.
[3] Suker M, Beumer BR, Sadot E, Marthey L, Faris JE, Mellon EA, et al. FOLFIRINOX for locally advanced pancreatic cancer: a systematic review and patient-level meta-analysis. Lancet Oncol 2016;17:801–10.
[4] Conroy T, Desseigne F, Ychou M, Bouché O, Guimbaud R, Bécouarn Y, et al. FOLFIRINOX versus gemcitabine for metastatic pancreatic cancer. N Engl J Med 2011;364:1817–25.
[5] Von Hoff DD, Ervin T, Arena FP, Chiorean EG, Infante J, Moore M, et al. Increased survival in pancreatic cancer with nab-paclitaxel plus gemcitabine. N Engl J Med 2013;369:1691–703.
[6] Kurdziel KA, Kalen JD, Hirsch JI, Wilson JD, Bear HD, Logan J, et al. Human dosimetry and preliminary tumor distribution of ^{18}F-fluoropaclitaxel in healthy volunteers and newly diagnosed breast cancer patients using PET/CT. J Nucl Med 2011;52:1339–45.
[7] Swayden M, Iovanna J, Soubeyran P. Pancreatic cancer chemo-resistance is driven by tumor phenotype rather than tumor genotype. Heliyon 2018;4:e01055.
[8] Schober M, Jesenofsky R, Faissner R, Weidenauer C, Hagmann W, Michl P, et al. Desmoplasia and chemoresistance in pancreatic cancer. Cancers (Basel) 2014;6:2137–54.
[9] Fukumura D, Jain RK. Tumor microenvironment abnormalities: causes, consequences, and strategies to normalize. J Cell Biochem 2007;101:937–49.
[10] Whatcott C, Han H, Posner RG, Von Hoff DD. Tumor–stromal interactions in pancreatic cancer. Crit Rev Oncog 2013;18:135–51.
[11] Ho WJ, Jaffee EM, Zheng L. The tumour microenvironment in pancreatic cancer — clinical challenges and opportunities. Nat Rev Clin Oncol 2020;17:527–40.
[12] Snipstad S, Mørch Ý, Sulheim E, Aslund A, Pedersen A, Davies CL, et al. Sonopermeation enhances uptake and therapeutic effect of free and encapsulated cabazitaxel. Ultrasound Med Biol 2021;47:1319–33.
[13] van Wamel A, Sontum PC, Healey A, Kvåle S, Bush N, Bamber J, et al. Acoustic Cluster Therapy (ACT) enhances the therapeutic efficacy of paclitaxel and Abraxane® for treatment of human prostate adenocarcinoma in mice. J Control Release 2016;236:15–21.
[14] Huang P, Zhang Y, Chen J, Shentu W, Sun Y, Yang Z, et al. Enhanced antitumor efficacy of ultrasonic cavitation with up-sized microbubbles in pancreatic cancer. Oncotarget 2015;6:20241–51.
[15] Kotopoulis S, Delalande A, Popa M, Mamaeva V, Dimcevski G, Gilja OH, et al. Sonoporation-enhanced chemotherapy significantly reduces primary tumour burden in an orthotopic pancreatic cancer xenograft. Mol Imaging Biol 2014;16:53–62.
[16] Bressand D, Novell A, Girault A, Raoul W, Fromont-Hankard G, Escoffre JM, et al. Enhancing nab-paclitaxel delivery using microbubble-assisted ultrasound in a pancreatic cancer model. Mol Pharm 2019;16:3814–22.
[17] Schultz CW, Ruiz de Garibay G, Langer A, Liu JB, Dhir T, Leitch C, et al. Selecting the optimal parameters for sonoporation of pancreatic cancer in a pre-clinical model. Cancer Biol Ther 2021;22:204–15.
[18] Gao J, Logan KA, Nesbitt H, Callan B, McKaig T, Taylor M, et al. A single microbubble formulation carrying 5-fluorouridine, irinotecan and oxaliplatin to enable FOLFIRINOX treatment of pancreatic and colon cancer using ultrasound targeted microbubble destruction. J Control Release 2021;338:358–66.
[19] Stride EP, Coussios CC. Cavitation and contrast: the use of bubbles in ultrasound imaging and therapy. Proc Inst Mech Eng H 2010;224:171–91.
[20] Lentacker I, De Cock I, Deckers R, De Smedt SC, Moonen CT. Understanding ultrasound induced sonoporation: definitions and underlying mechanisms. Adv Drug Deliv Rev 2014;72:49–64.
[21] Pitt WG, Husseini GA, Staples BJ. Ultrasonic drug delivery—a general review. Expert Opin Drug Deliv 2004;1:37–56.
[22] Snipstad S, Vikedal K, Maardalen M, Kurbatskaya A, Sulheim E, Davies CL. Ultrasound and microbubbles to beat barriers in tumors: improving delivery of nanomedicine. Adv Drug Deliv Rev 2021;177:113847.
[23] Dayton P, Klibanov A, Brandenburger G, Ferrara K. Acoustic radiation force in vivo: a mechanism to assist targeting of microbubbles. Ultrasound Med Biol 1999;25:1195–201.
[24] Hernot S, Klibanov AL. Microbubbles in ultrasound-triggered drug and gene delivery. Adv Drug Deliv Rev 2008;60:1153–66.
[25] Frenkel V. Ultrasound mediated delivery of drugs and genes to solid tumors. Adv Drug Deliv Rev 2008;60:1193–208.
[26] Afadzi M, Myhre OF, Yemane PT, Bjorkoy A, Torp SH, van Wamel A, et al. Effect of acoustic radiation force on the distribution of nanoparticles in solid tumors. IEEE Trans Ultrason Ferroelectr Freq Control 2021;68:432–45.
[27] Dimcevski G, Kotopoulis S, Bjanes T, Hoem D, Schjot J, Gjertsen BT, et al. A human clinical trial using ultrasound and microbubbles to enhance gemcitabine treatment of inoperable pancreatic cancer. J Control Release 2016;243:172–81.
[28] Mazur PK, Herner A, Neff F, Siveke JT. Current methods in mouse models of pancreatic cancer. Methods Mol Biol 2015;1267:185–215.
[29] Erstad DJ, Sojoodi M, Taylor MS, Ghoshal S, Razavi AA, Graham-O'Regan KA, et al. Orthotopic and heterotopic murine models of pancreatic cancer and their different responses to FOLFIRINOX chemotherapy. Dis Model Mech 2018;11:dmm034793.
[30] Freireich EJ, Gehan EA, Rall DP, Schmidt LH, Skipper HE. Quantitative comparison of toxicity of anticancer agents in mouse, rat, hamster, dog, monkey, and man. Cancer Chemother Rep 1966;50:219–44.
[31] National Center for Biotechnology Information. PubChem compound summary for CID 9887053, oxaliplatin. Bethesda, MD: Author; 2022.
[32] Lévi F, Metzger G, Massari C, Milano G. Oxaliplatin: pharmacokinetics and chronopharmacological aspects. Clin Pharmacokinet 2000;38:1–21.
[33] Campbell F, Verbeke CS. Pathology of the pancreas. London: Springer; 2013. p. 11–161.
[34] Stylianopoulos T, Munn LL, Jain RK. Reengineering the physical microenvironment of tumors to improve drug delivery and efficacy: from mathematical modeling to bench to bedside. Trends Cancer 2018;4:292–319.
[35] Kooiman K, Roovers S, Langeveld SAG, Kleven RT, Dewitte H, O'Reilly MA, et al. Ultrasound-responsive cavitation nuclei for therapy and drug delivery. Ultrasound Med Biol 2020;46:1296–325.
[36] Chen H, Kreider W, Brayman AA, Bailey MR, Matula TJ. Blood vessel deformations on microsecond time scales by ultrasonic cavitation. Phys Rev Lett 2011;106:034301.
[37] Chen H, Brayman AA, Matula TJ. Characteristic microvessel relaxation timescales associated with ultrasound-activated microbubbles. Appl Phys Lett 2012;101:163704.
[38] Theek B, Baues M, Ojha T, Möckel D, Veettil SK, Steitz J, et al. Sonoporation enhances liposome accumulation and penetration in tumors with low EPR. J Control Release 2016;231:77–85.

[39] Olsman M, Sereti V, Andreassen K, Snipstad S, van Wamel A, Eliasen R, et al. Ultrasound-mediated delivery enhances therapeutic efficacy of MMP sensitive liposomes. J Control Release 2020;325:121–34.
[40] Eggen S, Afadzi M, Nilssen EA, Haugstad SB, Angelsen B, de L Davies C. Ultrasound improves the uptake and distribution of liposomal doxorubicin in prostate cancer xenografts. Ultrasound Med Biol 2013;39:1255–66.
[41] Snipstad S, Hak S, Baghirov H, Sulheim E, Mørch Ý, Lélu S, et al. Labeling nanoparticles: dye leakage and altered cellular uptake. Cytometry A 2017;91:760–6.
[42] Liang C, Shi S, Meng Q, Liang D, Ji S, Zhang B, et al. Do anti-stroma therapies improve extrinsic resistance to increase the efficacy of gemcitabine in pancreatic cancer? Cell Mol Life Sci 2018;75:1001–12.
[43] Minchinton AI, Tannock IF. Drug penetration in solid tumours. Nat Rev Cancer 2006;6:583–92.
[44] Au JL, Yeung BZ, Wientjes MG, Lu Z, Wientjes MG. Delivery of cancer therapeutics to extracellular and intracellular targets: determinants, barriers, challenges and opportunities. Adv Drug Deliv Rev 2016;97:280–301.
[45] Tharkar P, Varanasi R, Wong WSF, Jin CT, Chrzanowski W. Nano-enhanced drug delivery and therapeutic ultrasound for cancer treatment and beyond. Front Bioeng Biotechnol 2019;7:324.
[46] Kalli M, Stylianopoulos T. Defining the role of solid stress and matrix stiffness in cancer cell proliferation and metastasis. Front Oncol 2018;8:55.
[47] National Center for Biotechnology Information. PubChem compound summary for CID 3385, fluorouracil. Bethesda, MD: Author; 2022.
[48] National Center for Biotechnology Information. PubChem compound summary for CID 60838, irinotecan. Bethesda, MD: Author; 2022.
[49] Gutiérrez ML, Muñoz-Bellvís L, Orfao A. Genomic heterogeneity of pancreatic ductal adenocarcinoma and its clinical impact. Cancers (Basel) 2021;13:4451.